Structure and Dynamics of Water on Forsterite Surface

Journal:	*Physical Chemistry Chemical Physics*
Manuscript ID	CP-ART-08-2018-005075.R1
Article Type:	Paper
Date Submitted by the Author:	09-Oct-2018
Complete List of Authors:	Liu, Tingting; The Ohio State University, School of Earth Sciences Gautam, Siddharth ; The Ohio State University, Wang, Hsiu-Wen; Joint Institue for Neutron Sciences, Anovitz, Lawrence; Oak Ridge National Laboratory, Chemical Sciences Division Mamontov, Eugene; Oak Ridge National Laboratory, Spallation Neutron Source Allard, Lawrence; Oak Ridge National Laboratory, High Temperature Materials Laboratory Microscopy Cole, David; The Ohio State University, School of Earth Sciences

Structure and Dynamics of Water on Forsterite Surface

Tingting Liu[a*†], Siddharth Gautam[a†], Hsiu-Wen Wang[b], Lawrence M Anovitz[b], Eugene Mamontov[c], Lawrence F Allard Jr[d], and David R Cole[a]

[a]*School of Earth Sciences, The Ohio State University, 125 South Oval Mall, Columbus, OH 43210*

[b]*Chemical Sciences Division, Oak Ridge National Laboratory, Oak Ridge, Tennessee 37831*

[c]*Neutron Scattering Science Division, Oak Ridge National Laboratory, Oak Ridge, Tennessee 37831*

[d]*Materials Science and Technology Division, Oak Ridge National Laboratory, Oak Ridge, Tennessee 37831*

**Corresponding author: Liu.2189@osu.edu*

†*These authors contributed equally to this work.*

Abstract: The behavior of water on mineral surfaces is the key to understanding interfacial and chemical reaction processes. Olivine is one of the major rock-forming minerals and its interaction with water is a ubiquitous phenomenon both on Earth's surface and in the subsurface. This work presents a combined study using molecular dynamics (MD) simulations and quasi-elastic neutron scattering (QENS) experiments conducted at three different instruments to study the structure and dynamics of water on forsterite (Mg- end member of olivine) surface at 270 K. The combination of three different QENS instruments probes dynamical processes occurring across broad time scales (~ 1 ps to ~ 1 ns in this study). The water structure on the hydroxylated surface is composed of three distinct water layers, transitioning from well-ordered and nearly immobile closest to the surface to a less structured layer. The energies of three motions (including translation and rotation) derived from simulations agree well with the experiments, covering the energy range from a few to hundreds of micro electron volts.

Introduction

The interaction and reaction of water with minerals control most of the chemical and transport processes encountered at the Earth's surface and subsurface ranging deep into the interior. The presence of water in other planetary bodies, comets and interstellar dust amplify the broad importance of water-mineral systems. Despite the extensive length and time scales over which these interactions can occur, there is the inescapable fact that interfacial phenomena - i.e., mineral surfaces as well as buried interfaces such as grain boundaries at the atomic scale - control the exchange of matter and energy that dictate the evolution of these systems.[1–3] One of the most important of these is the olivine-water system. Olivine-series minerals compose a major portion of Earth's upper mantle and oceanic crust, and are observed in lunar and Martian rocks. They are very susceptible to near-surface reactions involving water that are generally complex and lead to hydration, silicification, oxidation or carbonation.[4,5] Furthermore, olivine-water interactions are thought to be a major source of water during planetary accretion.[6,7]

The dominant olivine-series phase is forsterite which is the Mg- end member of a complete solid solution where magnesium and iron as cations substitute for each other ($[Mg,Fe]_2SiO_4$). Calorimetric measurements of the adsorption energy have been made on forsterite powder interacting with water.[8] A more recent experimental study observed the effects of water on the carbonation of forsterite with application to CO_2 sequestration.[9] To date, probing the structural and dynamical behavior of interfacial water on forsterite has been relegated to studies employing different molecular simulation methods. For example, Kerisit et al.[10] used classical molecular dynamics (MD) simulations to investigate water on forsterite surfaces, together with CO_2 under the condition of 50°C and 180 bar to simulate subsurface CO_2 sequestration. Their focus was on the form and transport of the supercritical CO_2 on the interface,

which depends on the water content. In a related study, Kerisit et al. used density functional theory (DFT) with dispersion corrections to examine adsorption of water on the (010) surfaces of five end members of olivine minerals ($[X]_2SiO_4$ where X = Mg, Ca, Mn, Fe, and Co).[11] Collectively, these and related molecular simulation studies[12–14] suggest that water on such surfaces can exhibit several dynamical processes occurring over a broad range of characteristic times.

In order to quantify the various types of molecular water motion on the surface of forsterite, we have conducted a series of quasi-elastic neutron scattering (QENS) experiments complemented by classical MD simulations. The exceptionally large incoherent neutron scattering cross-section of hydrogen compared to that of other elements makes it an ideal technique to probe the dynamics of water, in particular, the self-diffusive motions.[15] Recent studies using MD simulations in concert with QENS data have demonstrated the power of integrating outcomes from the two approaches in quantifying the interfacial behavior of water on select metal oxide and mineral surfaces.[12–14,16]

Experiments and Simulations

The QENS experiments were carried out at the high flux backscattering spectrometer (HFBS)[17] and the disc chopper spectrometer (DCS)[18] at the NIST Center for Neutron Research (NCNR), and at the backscattering silicon spectrometer (BASIS)[19], Spallation Neutron Source (SNS) at the Oak Ridge National Laboratory (ORNL). The dynamic energy ranges are ±11 μeV, -1 ~ +0.2 meV, and ±100 μeV for HFBS, DCS, and BASIS, respectively, and their corresponding energy resolutions are 0.775 μeV, 10.9 μeV, and 3.3 μeV at their full width at half maximum (FWHM). Data affording the best opportunity for comparison was obtained at 270 K.

The sample loading and experimental setup are the same as described in Mamontov et al.[16] Synthetic nano-powdered forsterite[20] with a high surface area (66.0 m^2g^{-1}, more characterization images can be found in Fig. S1 in the Supporting Information) is placed in a vacuum oven and then equilibrated with water vapor at 150°C for hydration for 24h and at 50°C for outgassing the physisorbed water molecules afterwards. Fully hydrated forsterite sample (water content of ~ 10% wt. determined by thermogravimetric analysis, see Fig. S2 in the Supporting Information) was sealed in a flat aluminum cell and kept in the path of the neutron beam. To avoid multiple scattering, the thickness of the sample cell was chosen such that it allowed a neutron transmission of more than 90%. The three instruments have overlapping energy windows and resolution allowing for an investigation of relaxation times from ~ 1 ps to ~ 1 ns (Fig. S3 in the Supporting Information).

To complement the QENS measurements, we applied classical MD simulations using empirical force fields to investigate the structural and dynamical properties of water on a hydroxylated forsterite surface, which represents the real mineral surface at near-ambient conditions. MD simulations were performed using DL_POLY_4.06 package.[21] Among the common crystal planes of olivine mineral[22] in concert with material characteriztion for the synthetic nano-powdered forsterite (Fig. S1 in the Supporting Information), we selected the (010) surface because it is relatively stable with a lower surface energy, as evidenced by previous simulation studies.[7,23] There are two possible terminations of the forsterite(010) surface referred to as dipolar and non-dipolar[23], as shown in Fig. S4 of the Supporting Information. We selected the non-dipolar termination for our study, which is a reasonable choice as it has a lower surface energy than the dipolar termination. Furthermore, de Leeuw et al. have pointed out the non-dipolar hydroxylated (010) surface adsorbs molecular water more favorably than the dipolar

hydroxylated surface.[23] Thus this study employed the non-dipolar hydroxylated surface. The simulation box is composed of a forsterite slab (*Pbnm* space group, a = 4.753 Å, b= 10.199 Å, c = 5.981 Å, experimental unit cell determined by Lager et al.[24]) with a unit cell replicated 6 × 1.5 × 6 times (1512 atoms) and an additional free space (~ 85 Å) along the b-axis to allow 392 water molecules to move. Sec. SI in the Supporting Information indicates how this number of molecules is equivalent to the hydration layers achieved by experiments. This large spacing ensures that the surface effect dominates over the slit-pore confinement. Two sides of the surface are cleaved to be non-dipolar and Si-O tetrahedron is kept intact. More simulation details are presented in the Sec. SI of the Supporting Information.

Results and Discussion

Figs. 1a and 1b show the surface water structure and its corresponding density profile at 270 K obtained by MD simulations. Three layers of water molecules on the surface are visible in the density profile. The first layer (closest to the surface designated as L1) is formed by the interaction between water molecules and the surface OH and H groups. The higher density seen in Fig. 1b for L1 is due to the ordered structure, which is mainly controlled by the morphology of the hydroxylated surface. All the three layers render higher density than bulk water as shown in Fig. 1b. The second layer of water molecules (L2) interacts with L1 and the surface OH groups. The molecules in L2 are less ordered than L1, thus the density is lower. L1 and L2 span a total distance of ~ 2.5 Å. Beyond L2, the third layer of molecules (denoted as L3) interacts with L2 and each other in a disordered network. The maximum duration for molecules residing in L2 or L3 is described in Sec. SII of the Supporting Information. Fig. 1c shows trajectories of selected water molecules only residing in a particular layer for their maximum duration. Fig. 1d plots the trajectories perpendicular to the surface of two representative molecules that exhibit their

maximum duration in each layer over the entire production time period (1.5 ns). Molecules residing in L1 show very limited mobility based on their trajectories, while molecules in L2 and L3 are free to move and communicate between the two layers. In L2, molecules are less mobile than in L3. It is important to reiterate that L1, L2, and L3 represent separate interfacial layers occupied by a collection of molecules exhibiting similar structural and dynamical properties.

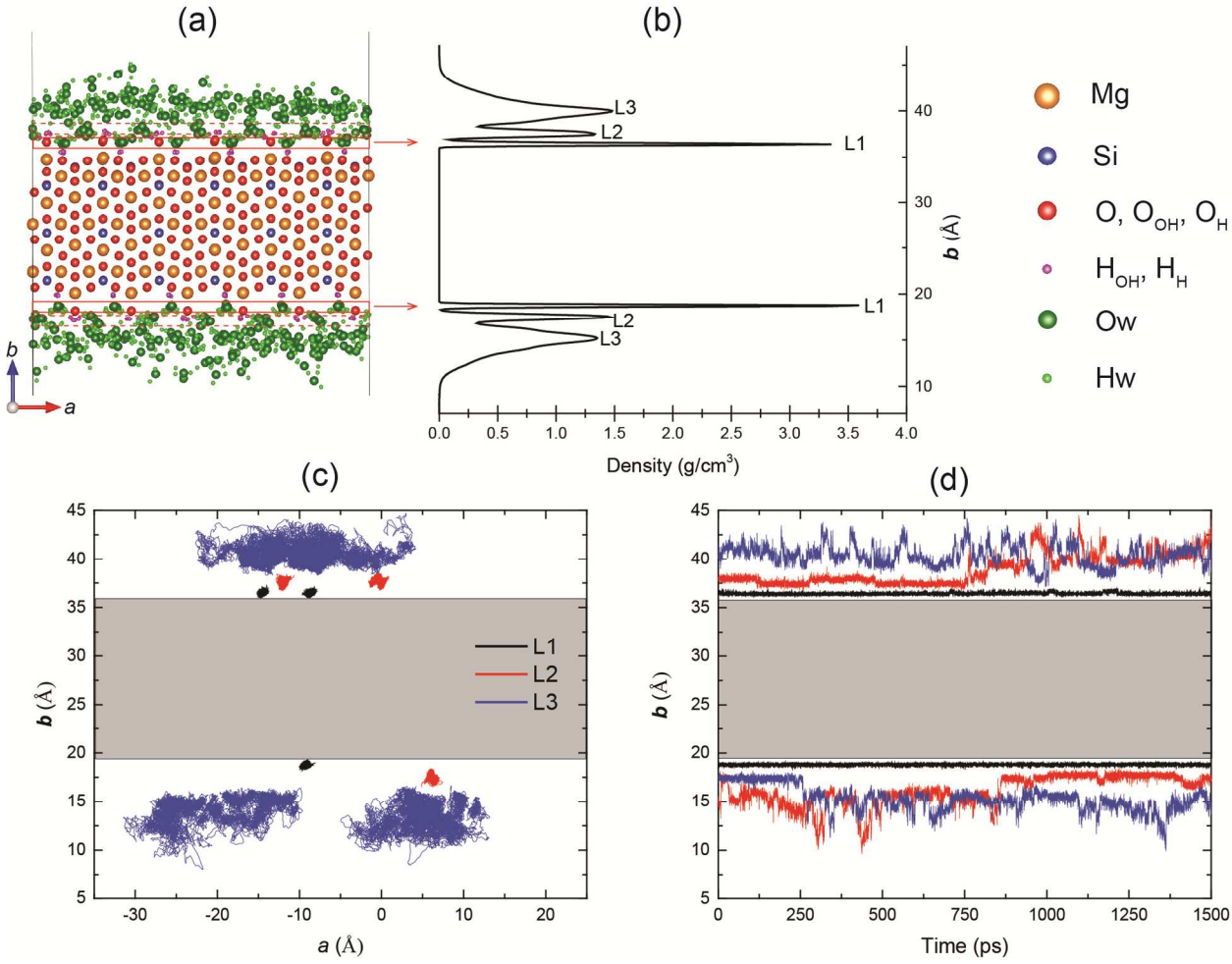

Fig. 1. (a) A snapshot of water molecules on hydroxylated forsterite(010) surface at 270 K. The highlighted areas with boxes indicate L1 (solid red line) and L2 (dashed red line). (b) Corresponding density profile for adsorbed water molecules. (c) Trajectories of four representative molecules residing in L1, L2, L3 along *a*-*b* plane. (d) Trajectories perpendicular to the surface over time using two molecules from L1, L2 and L3. The forsterite slab is shown as a grey rectangle.

Mean squared displacement (MSD) is used to describe the translational diffusive motion of molecules. The diffusion coefficient (D) determined from MSD is based on the Einstein relation:

$$D = \frac{MSD}{6t} \quad (1)$$

The D value determined for water on the forsterite surface is 0.42×10^{-9} m^2s^{-1}. Using MD simulations, Lee and Rossky placed water with a density of 0.9963 $g \cdot cm^{-3}$ at 25°C on three type of surfaces, i.e., a flat hydrophobic surface, a rough hydrophobic surface, and a hydrophilic silica surface, and obtained the water diffusion coefficients of ~ 3.5×10^{-9} m^2s^{-1}, ~ 2.7×10^{-9} m^2s^{-1}, ~ 0.96×10^{-9} m^2s^{-1}, respectively.[25] The value of D in our study is comparable to the hydrophilic surface mentioned above, as a hydroxylated surface is expected to strongly interact with water molecules. Details about MSD of water molecules residing in different layers can be found in Fig. S5 in the Supporting Information. Using the trajectory of molecules residing only in L3, the diffusion coefficient is calculated to be 0.58×10^{-9} m^2s^{-1}, which is smaller than that of bulk water calculated in this study (2.39×10^{-9} m^2s^{-1} at 298 K). Related to the higher density than bulk water shown in Fig. 1b, a lower D value can be expected.

The QENS data collected from the three instruments were reduced using the data analysis package DAVE.[26] Representative reduced spectra converted to the dynamical structure factor $S(\boldsymbol{Q},\omega)$ are shown in Fig. 2. $S(\boldsymbol{Q},\omega)$ is a property of the sample and is a function of momentum ($\hbar\boldsymbol{Q}$) and energy transferred ($\hbar\omega$) between the neutron and the sample in a scattering event and thus records information on the structure and dynamics of the sample. It is noted that the $S(\boldsymbol{Q},\omega)$ in these experiments represents the incoherent dynamical structure factor of adsorbed water because the incoherent neutron scattering cross-section of hydrogen dominates the scattering.

An attempt to fit the quasi-elastic broadening (qe) with a single Lorentzian function did not result in satisfactory fits. Therefore, a combination of two Lorentzians was used to model the qe broadening. The whole spectra were thus fit using the equation shown below:

$$S(Q,\omega) = \left\{ A(Q)\delta(\omega) + \left[1 - A(Q)\right]\left[pL_1(\Gamma_1,\omega) + (1-p)L_2(\Gamma_2,\omega)\right] + \left[B_1 + B_2(Q,\omega)\right]\right\} \otimes R(Q,\omega) \quad (2)$$

The elastic signal $A(\boldsymbol{Q})$, two Lorentzian components $L_1(\Gamma_1,\omega)$ and $L_2(\Gamma_2,\omega)$ (p as the prefactor), and a linear background $B_1+B_2(\boldsymbol{Q},\omega)$ are convoluted by the resolution function $R(\boldsymbol{Q},\omega)$. The elastic signal derived from motions slower than the resolution of the instrument and weak scattering from the forsterite are modeled using a convoluted delta function ($\delta(\omega)$) centered on zero energy transfer. The quasi-elastic components, modeled by the Lorentzian functions, are separated into a fast and slow component on the time scale of the instrument (HFBS only allows one Lorentzian fitting due to its narrow energy range, see Figs. 2a, 2b). By fitting the spectra with eqn (2), we determined the parameters A, p, and the half width at half maximum (HWHM) of the two Lorentzians, Γ_i^e (e denotes experiment, i = 1, 2). Good quality fits were obtained in this manner as seen in Fig. 2 where the individual components along with the overall fit function described in eqn (2) are shown together with the experimental spectra. The two Lorentzians representing the qe broadening have different HWHM that correspond to different time scales of motion, denoted as "fast" and "slow" hereafter. Here the designation of "fast" and "slow" is limited to the energies accessible at one instrument. Both BASIS and DCS have their own "fast" and "slow" components and due to an overlap of the energies accessible at these instruments, the "fast" component of BASIS might be comparable to the "slow" component of DCS. Fitted parameters A and p among the instruments are described in Fig. S11 in the Supporting Information. In Fig. S11, the variation of A parameter with $\boldsymbol{Q}$ suggests the presence of a localized

184 motion; and *p* values indicate that in the BASIS spectra the fast component dominates, whereas
185 in the DCS the slower one dominates, both of which fall in the intermediate dynamic range.
186 Detailed analysis can be found in the Supporting Information.

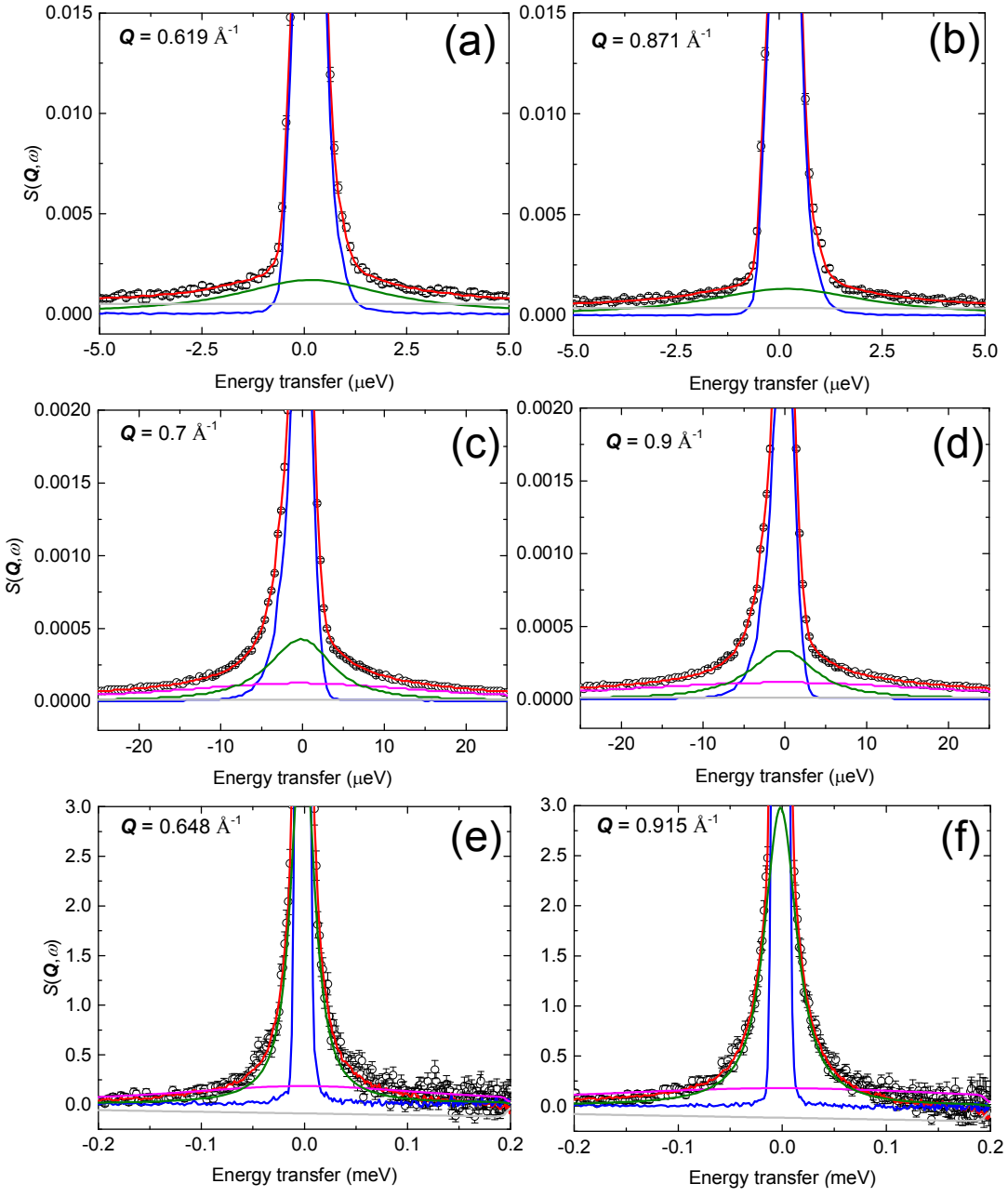

187

188 Fig. 2. Representative QENS spectra obtained at 270 K at HFBS (a, b), BASIS (c, d) and DCS (e,
189 f). Experimental data are represented by hollow circles. Total fit function is shown in red (–);

elastic component in blue (–); two Lorentzian components in magenta (–) and green (–), and background in light grey (–). Spectra are shown in limited quasi-elastic energy range for clarity.

Normally, a comparison is made between the diffusion coefficients obtained from QENS experiments and those obtained using MSD from MD simulations. However, MSD is a function of time alone and does not discriminate between motions at different length scales, thus it might incorporate motions occurring at length and time scales that are beyond the energy window of the instruments.[27] A more direct comparison between the simulations and QENS experiments can be made by calculating the intermediate scattering function (ISF, $I(\boldsymbol{Q},t)$) that is the inverse Fourier transform of the dynamic structure factor $S(\boldsymbol{Q},\omega)$ measured in the QENS experiment. Several such direct comparisons have been attempted.[28–30] In an MD simulation, the ISF can be calculated as

$$I(Q,t) = \frac{1}{N}\sum_i \langle e^{i\boldsymbol{Q}\cdot(r_i(t)-r_i(0))}\rangle \quad (3)$$

where $\boldsymbol{Q}$ is the momentum transfer, and $\boldsymbol{r_i}$ is the position vector of the ith hydrogen atom in the simulation. The summation is over hydrogen atoms of all water molecules. The angular brackets denote an ensemble average and integrate the contribution from $\boldsymbol{Q}$ in all directions with the same magnitude. Fig. 3 shows the calculated ISF function from one example $\boldsymbol{Q}$ value (= 0.525 Å^{-1}) at 270 K using trajectories of 1.5 ns. Another simulation with 10 ns production run after 20 ns of equilibration was carried out to confirm if 1.5 ns production run is sufficient to produce converged quantities. ISF and MSD calculated from this longer simulation of 10 ns yielded very close results to those calculated from 1.5 ns simulation. (see in Fig. S6 in the Supporting Information). Because experimental $S(\boldsymbol{Q},\omega)$ profiles were modeled with combinations of Lorentzian functions, the corresponding ISF calculated from the simulation can be modeled by a

combination of exponential functions.[27] In order to model the total ISF over the entire time range, a function composed of three exponential functions and a constant is employed:

$$I(Q,t) = A_1 e^{-t/\tau_1} + A_2 e^{-t/\tau_2} + A_3 e^{-t/\tau_3} + c \quad (4)$$

where τ_1, τ_2, and τ_3 are the decay times that define three distinct decay stages. The fitting curve in Fig. 3 is the result of fitting calculated ISF data using eqn (4). The three exponential decay terms in eqn (4), when inverse Fourier transformed, would result in three Lorentzian functions $L_i^s(\Gamma_i^s,\omega)$ (i=1, 2, 3) with HWHM (Γ_i^s) related to the corresponding decay times according to the relation

$$\Gamma_i^s = \frac{\hbar}{\tau_i} \quad (5)$$

where s denotes simulation. The Lorentzians $L_i^s(\Gamma_i^s,\omega)$ represent the same quantities as the experiment-derived Lorentzians $L_i^e(\Gamma_i,\omega)$ (i=1, 2) in eqn (2) and are amenable to direct comparison. The four components of the fit (three Lorentzians and one constant) are also plotted in Fig. 3. In addition, the trajectories of ten representative molecules from L1, L2 and L3 with a certain time period facilitates the respective layer-specific ISF which are also shown in Fig. 3.

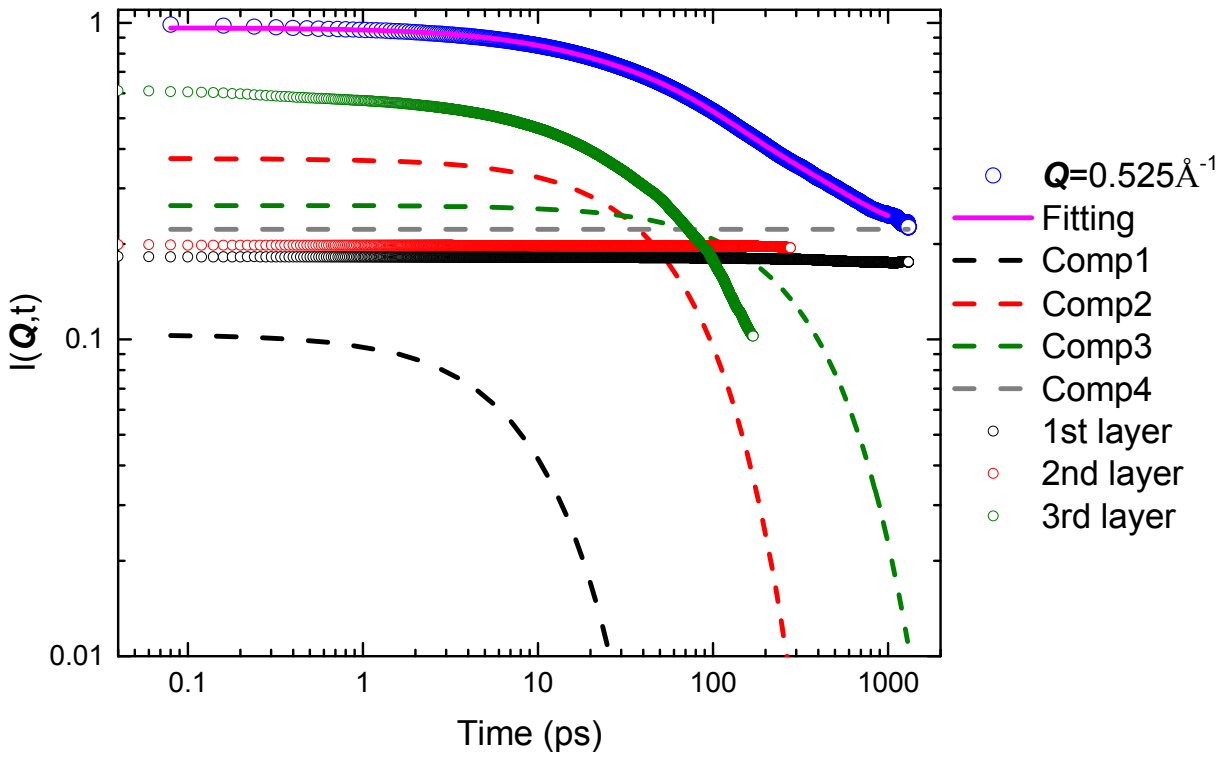

Fig. 3. Calculated total ISF using one ***Q*** value at 270 K and fitting curve obtained using eqn (4). Four components in eqn (4) are plotted in dashed lines. The ISF curves representing L1, L2 and L3 are represented by open circles.

In Fig. 3, the three exponential decay components of the fit (dashed lines) show different decaying rates; however, the constant component represents extremely slow motions that may remain unresolved in an experiment due to the finite resolution of the instrument used. This slow motion matches the characteristics of the molecules in L1 and L2 (black and red circles), which show restricted mobility. Only molecules in L3 exhibit motions that can be described on the time scales of the three exponential components used to fit the overall ISF. The ISF calculated for L3 (green circles) can be fitted by a linear combination of these three exponentials (Fig. S7 in the Supporting Information). From the weight percentage of the three exponentials in the fits to the L3 ISF, we conclude that the intermediate time scale with a τ_2 value of 73 ps dominates the dynamics in L3. Mamontov et al. examined the dynamics of molecular water on the TiO_2(110)

surface using QENS and MD, and found that while the chemisorbed water in L1 is too slow to be observed in their experiment, water molecules in both the (L2+L3) above this L1 contributed to the experimental spectra.[12]

In addition, average residence time (τ_R), a measure of how long a typical molecule remains in a given region of space,[31,32] was also estimated for all the three layers (Fig. S10 in the Supporting Information). Estimates for the average residence time are 956 ps, 49.5 ps, and 335 ps for L1, L2, and L3, respectively. The motions of molecules in L1 are severely restricted, thus the τ_R is longer for L1 than that for the other two layers. Due to the thicknesses of L2 and L3 shown in Fig. 1b, we can expect the molecules in L2 have shorter τ_R and easily move beyond the narrow region and molecules in L3 experience a longer time to escape the thicker layer.

Fig. 4 compares the Γ_i values obtained by fitting the experimental QENS spectra using eqn (2) and those obtained from eqn (4) by converting the decay constants of exponentials derived from ISF fitting from the simulations. In Fig. 4, we observe the three components (Γ_1^s, Γ_2^s, Γ_3^s) determined by simulation span a wide energy range, whose HWHM ranges from a few to hundreds of μeV. Each component matches the combination of motion from different instruments, which is due to the specific energy range accessible at the instrument. In the three energy domains in Fig. 4, the fastest component (Γ_1^s) from simulation matches the fast component observed on DCS; the intermediate component (Γ_2^s) matches the fast component observed on BASIS and the slow component from DCS; and the slowest component (Γ_3^s) matches the slow component from BASIS and the single component from HFBS. We observe that Γ_1^s becomes much faster in higher $\boldsymbol{Q}$ region. However, in the $\boldsymbol{Q}$ range that is consistent with

DCS fast component, the simulation and experimental data agree well. The slowest component Γ_3^s, crosses two sets of data (BASIS-slow and HFBS); however, the agreement is still reasonable given that the energy range is narrow in this domain. The intermediate component Γ_2^s agrees well with the experimental data, in particular with the DCS-slow.

A comparison of simulation and experimental results in Fig. 4 demonstrates a close match between Γ_2^s and the experimental intermediate components (BASIS-fast and DCS-slow). As shown above, the contribution to these spectra comes from L3 alone and Γ_2^s dominates the dynamics in L3. The above agreement is confirmed again by the analysis of the *p* parameter, which indicates that BASIS-fast and DCS-slow components dominate the quasi-elastic signal (see Fig. S11b in the Supporting Information). Temperatures of 285 K and 300 K were also investigated by BASIS, and the dynamics at 300 K is faster than 270 K by a factor of ~ 1.5, with a similar trend shared by all three temperatures (see Fig. S12 in the Supporting Information).

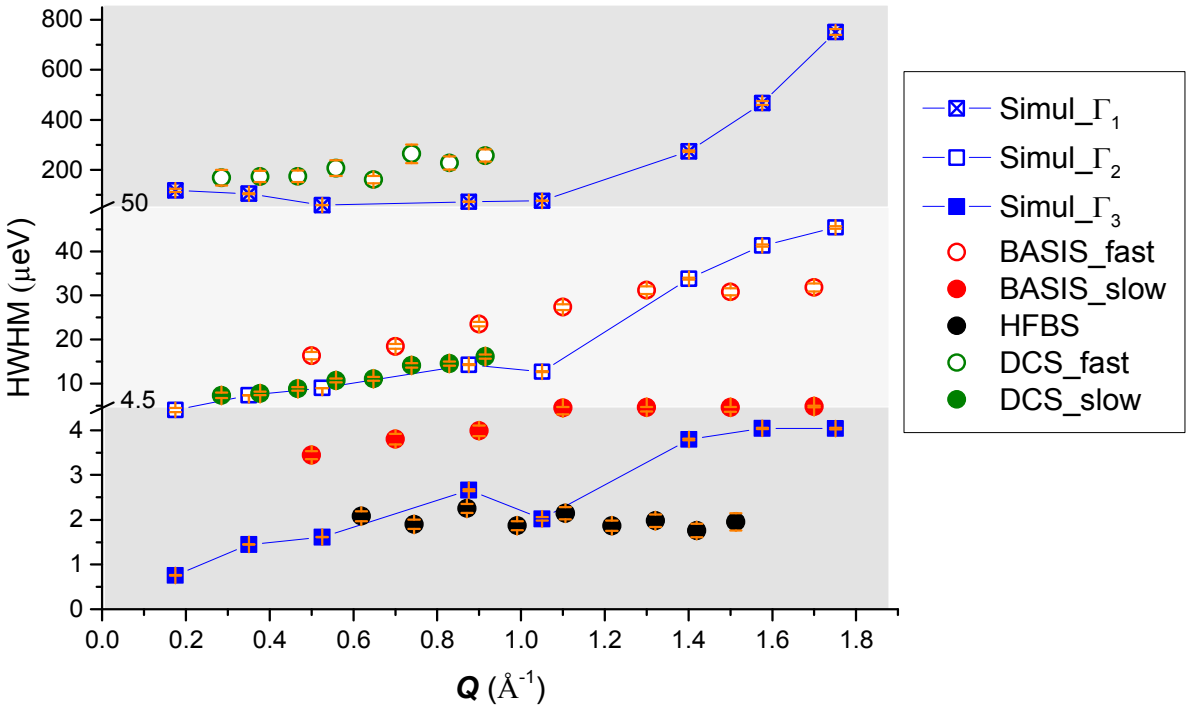

Fig. 4. Comparison of the QENS data with MD simulation data. Three representative energy domains are outlined in grey areas. All the error bars are shown in orange.

Rotational behavior observed from the second and third stages of decay of the rotational ISF (see Fig. S9 in the Supporting Information) suggest the corresponding time scales are within the ranges accessible at DCS and BASIS. Therefore, the quasi-elastic broadening observed in the DCS and BASIS spectra can be expected to have a contribution from the rotational motion of water. This is consistent with A values whose trends with $\boldsymbol{Q}$ indicates localized motion in the experimental spectra (see Fig. S11a in the Supporting Information).

Conclusions

In conclusion, this study examines structure and dynamics of water on hydroxylated forsterite(010) surface at 270 K using MD simulation and QENS experiments. The density profile indicates water molecules on the surface compose three distinct layers: L1+L2 include nearly immobile molecules with relatively less structural disorder in L2; and L3 is composed of disordered water molecules. Motion of water on the forsterite surface consists of several dynamical processes that occur at different time scales. The ISF calculated from the simulations can be described by four components that represent motions at different time scales. Out of these four, the energies associated with three components match the energies of three components of motions observed in the QENS experiments. Simulation results indicate water molecules in L3 are primarily responsible for the observable dynamics, while the restricted molecules in L1+L2 cannot be detected by the experiments. We have provided an excellent example of how MD simulation in concert with neutron scattering experimental data provides precise and complementary information for understanding the structure and dynamics of water on a mineral surface.

Conflicts of interest

Authors do not declare any conflict of interest.

Acknowledgements

We want to thank the two anonymous reviewers whose comments greatly improve the quality of the work. This material is based upon work supported by the U.S. Department of Energy, Office of Science, Office of Basic Energy Sciences, Division of Chemical Sciences, Geosciences and Biosciences, Geosciences Program (T.L. and S.G. were supported under grant DESC0006878 to Ohio State University). T.L. also thanks the computing resources provided by the Deep Carbon Observatory cluster hosted by Rensselaer Polytechnic Institute. We acknowledge the support of the National Institute of Standards and Technology, U.S. Department of Commerce, in providing the neutron research facilities used in this work. Access to DCS and HFBS was provided by the Center for High Resolution Neutron Scattering, a partnership between the National Institute of Standards and Technology and the National Science Foundation under Agreement No. DMR-1508249. The neutron scattering experiments at Oak Ridge National Laboratory's (ORNL) Spallation Neutron Source were supported by the Scientific User Facilities Division, Office of Basic Energy Sciences, U.S. Department of Energy (DOE).

References

1 A. Lüttge and R. S. Arvidson, in *Kinetics of Water-Rock Interaction*, eds. S. L. Brantley, J. D. Kubicki and A. F. White, Springer New York, New York, NY, 2008, pp. 73–107.

2 A. Striolo, From Interfacial Water to Macroscopic Observables: A Review, *Adsorpt. Sci. Technol.*, 2011, **29**, 211–258.

3 C. V. Putnis and E. Ruiz-Agudo, The Mineral-Water Interface: Where Minerals React with the Environment, *Elements*, 2013, **9**, 177–182.

4 M. A. Velbel, Dissolution of olivine during natural weathering, *Geochim. Cosmochim. Acta*, 2009, **73**, 6098–6113.

5 M. J. Wilson, Weathering of the primary rock-forming minerals: processes, products and rates, *Clay Miner.*, 2004, **39**, 233–266.

6 H. E. King, M. Stimpfl, P. Deymier, M. J. Drake, C. R. A. Catlow, A. Putnis and N. H. de Leeuw, Computer simulations of water interactions with low-coordinated forsterite surface sites: Implications for the origin of water in the inner solar system, *Earth Planet. Sci. Lett.*, 2010, **300**, 11–18.

7 M. Stimpfl, A. M. Walker, M. J. Drake, N. H. de Leeuw and P. Deymier, An ångström-

sized window on the origin of water in the inner solar system: Atomistic simulation of adsorption of water on olivine, *J. Cryst. Growth*, 2006, **294**, 83–95.

8 S. Chen and A. Navrotsky, Calorimetric study of the surface energy of forsterite, *Am. Mineral.*, 2009, **95**, 112–117.

9 C. J. Thompson, P. F. Martin, J. Chen, P. Benezeth, H. T. Schaef, K. M. Rosso, A. R. Felmy and J. S. Loring, Automated high-pressure titration system with in situ infrared spectroscopic detection, *Rev. Sci. Instrum.*, 2014, **85**, 044102.

10 S. Kerisit, J. H. Weare and A. R. Felmy, Structure and dynamics of forsterite–scCO2/H2O interfaces as a function of water content, *Geochim. Cosmochim. Acta*, 2012, **84**, 137–151.

11 S. Kerisit, E. J. Bylaska and A. R. Felmy, Water and carbon dioxide adsorption at olivine surfaces, *Chem. Geol.*, 2013, **359**, 81–89.

12 E. Mamontov, D. J. Wesolowski, L. Vlcek, P. T. Cummings, J. Rosenqvist, W. Wang and D. R. Cole, Dynamics of Hydration Water on Rutile Studied by Backscattering Neutron Spectroscopy and Molecular Dynamics Simulation, *J. Phys. Chem. C*, 2008, **112**, 12334–12341.

13 A. G. Stack, J. M. Borreguero, T. R. Prisk, E. Mamontov, H.-W. Wang, L. Vlcek and D. J. Wesolowski, Precise determination of water exchange on a mineral surface, *Phys. Chem. Chem. Phys.*, 2016, **18**, 28819–28828.

14 L. J. Michot, A. Delville, B. Humbert, M. Plazanet and P. Levitz, Diffusion of Water in a Synthetic Clay with Tetrahedral Charges by Combined Neutron Time-of-Flight Measurements and Molecular Dynamics Simulations, *J. Phys. Chem. C*, 2007, **111**, 9818–9831.

15 M. Bee, M. Foulon, J. P. Amoureux, C. Caucheteus and C. Poinsignon, The glassy phase of 1-cyanoadamantane; a study of the molecular reorientations by high-resolution quasi-elastic neutron scattering, *J. Phys. C Solid State Phys.*, 1987, **20**, 337–349.

16 E. Mamontov, L. Vlcek, D. J. Wesolowski, P. T. Cummings, W. Wang, L. M. Anovitz, J. Rosenqvist, C. M. Brown and V. G. Sakai, Dynamics and Structure of Hydration Water on Rutile and Cassiterite Nanopowders Studied by Quasielastic Neutron Scattering and Molecular Dynamics Simulations, *J. Phys. Chem. C*, 2007, **111**, 4328–4341.

17 A. Meyer, R. M. Dimeo, P. M. Gehring and D. A. Neumann, The high-flux backscattering spectrometer at the NIST Center for Neutron Research, *Rev. Sci. Instrum.*, 2003, **74**, 2759–2777.

18 J. R. D. Copley and J. C. Cook, The Disk Chopper Spectrometer at NIST: a new instrument for quasielastic neutron scattering studies, *Chem. Phys.*, 2003, **292**, 477–485.

19 E. Mamontov and K. W. Herwig, A time-of-flight backscattering spectrometer at the Spallation Neutron Source , BASIS, *Rev. Sci. Instrum.*, 2011, **82**, 085109.

20 L. M. Anovitz, A. J. Rondinone, L. Sochalski-kolbus, J. Rosenqvist and M. C. Cheshire,

Nano-scale synthesis of the complex silicate minerals forsterite and enstatite, *J. Colloid Interface Sci.*, 2017, **495**, 94–101.

21 I. T. Todorov, W. Smith, K. Trachenko and M. T. Dove, DL_POLY_3: new dimensions in molecular dynamics simulations via massive parallelism, *J. Mater. Chem.*, 2006, **16**, 1911–1918.

22 W. A. Deer, R. A. Howie and J. Zussman, Eds., *Rock-forming minerals: Vol. 1A. Orthosilicates*, Geological Society Publishing House, London, 2nd edn., 1997.

23 N. H. de Leeuw, S. C. Parker, C. R. a. Catlow and G. D. Price, Modelling the effect of water on the surface structure and stability of forsterite, *Phys. Chem. Miner.*, 2000, **27**, 332–341.

24 G. A. Lager, F. K. Ross, F. J. Rotella and J. D. Jorgensen, Neutron powder diffraction of forsterite, Mg2SiO4: a comparison with single-crystal investigation, *J. Appl. Cryst.*, 1981, **14**, 137–139.

25 S. H. Lee and P. J. Rossky, A comparison of the structure and dynamics of liquid water at hydrophobic and hydrophilic surfaces—a molecular dynamics simulation study, *J. Chem. Phys.*, 1994, **100**, 3334–3345.

26 R. T. Azuah, L. R. Kneller, Y. Qiu, P. L. W. Tregenna-Piggott, C. M. Brown, J. R. D. Copley and R. M. Dimeo, DAVE : A Comprehensive Software Suite for the Rduction, Visualization, and Analysis of Low Energy Neutron Spectroscopic Data, *J. Res. Natl. Inst. Stand. Technol.*, 2009, **114**, 341–358.

27 S. Gautam, T. Le, A. Striolo and D. Cole, Molecular dynamics simulations of propane in slit shaped silica nano-pores: direct comparison with quasielastic neutron scattering experiments, *Phys. Chem. Chem. Phys.*, 2017, **19**, 32320–32332.

28 N. Morelon, G. R. Kneller, M. Ferrand, A. Grand, J. C. Smith and M. Bée, Dynamics of alkane chains included in an organic matrix: Molecular dynamics simulation and comparison with neutron scattering experiment, *J. Chem. Phys.*, 1998, **109**, 2883–2894.

29 S. Gautam, S. Mitra, R. Mukhopadhyay and S. L. Chaplot, Diffusion of acetylene inside Na-Y zeolite: Molecular dynamics simulation studies, *Phys. Rev. E*, 2006, **74**, 041202.

30 S. Gautam, S. Mitra, S. L. Chaplot and R. Mukhopadhyay, Dynamics of 1,3-butadiene adsorbed in Na-Y zeolite: A molecular dynamics simulation study, *Phys. Rev. E*, 2008, **77**, 061201.

31 S. Kerisit, E. S. Ilton and S. C. Parker, Molecular Dynamics Simulations of Electrolyte Solutions at the (100) Goethite Surface, *J. Phys. Chem. B*, 2006, **110**, 20491–20501.

32 U. Terranova and N. H. de Leeuw, Structure and dynamics of water at the mackinawite (001) surface, *J. Chem. Phys.*, 2016, **144**, 094706.